

Unusual Fermi surface nesting in parent compounds of iron arsenic high temperature superconductors revealed by Angle Resolved Photoemission Spectroscopy

Takeshi Kondo,¹ R. M. Fernandes,¹ R. Khasanov,² Chang Liu,¹ A. D. Palczewski,¹ Ni Ni,¹ M. Shi,³ A. Bostwick,⁴ E. Rotenberg,⁴ J. Schmalian,¹ S. L. Bud'ko,¹ P. C. Canfield,¹ and A. Kaminski¹

¹*Ames Laboratory and Department of Physics and Astronomy, Iowa State University, Ames, Iowa 50011, USA*

²*Laboratory for Muon Spin Spectroscopy, Paul Scherrer Institut, CH-5232 Villigen PSI, Switzerland*

³*Swiss Light Source, Paul Scherrer Institut, CH-5232 Villigen PSI, Switzerland*

⁴*Advanced Light Source, Berkeley National Laboratory, Berkeley, California 94720, USA*

(Dated: November 29, 2018)

We use angle resolved photoemission spectroscopy (ARPES) to study the band structure of BaFe_2As_2 and CaFe_2As_2 , two of the parent compounds of the iron arsenic high temperature superconductors. We find clear evidence for band back folding and hybridization demonstrating that conduction electrons are strongly affected by the emergence of magnetic order. Our high quality data revealed that although the Fermi surface is strongly three-dimensional, it does indeed have long parallel segments along the k_z direction that can lead to the emergence of magnetic order. More interestingly, we find very unusual incommensurate nesting of the Fermi surface in the $a - b$ plane that is present only at low temperatures. We speculate that this is a signature of a failed Charge Density Wave (CDW) state that was predicted by renormalization group studies.

PACS numbers: 79.60.-i, 74.25.Jb, 74.70.-b

Iron arsenic superconductors [1] display a fascinating interplay between magnetism and superconductivity. The influence of the magnetism on the electronic properties and the role it plays in high temperature superconductivity of these materials is a subject of a lively debate within the condensed matter physics community. Neutron scattering experiments[2, 3] reported antiferromagnetic (AF) ordering and 3D character of magnetic interactions[4] in non-doped parent compounds of iron arsenides. A number of previous studies attributed the magnetic ordering to itinerant Spin Density Wave (SDW) [5, 6, 7], while others favored magnetic order due to localized moments [8]. The AF-ordering is reminiscent of that of the cuprate high temperature superconductors, which occurs in the un-doped materials [9]. The AF ordering introduces a new zone boundary (antiferromagnetic zone boundary - AFZB) leading to band back folding effects [10, 11]. The main difference between the iron arsenides and cuprates is that the parent (undoped) phase in the former is not insulating but metallic [12, 13, 14, 15]. This opens the possibility of investigating the interplay between long range magnetic ordering and the conduction electrons. Understanding this interaction is essential to elucidate the origin of the fascinating properties displayed by the new, iron-arsenic based superconductors, and may also help to better understand the relation between magnetic and electronic excitations in the cuprates where we do not have access to a conducting, magnetically ordered state of the parent, undoped materials. In this letter, we present data from angle resolved photoemission spectroscopy (ARPES) on the electronic properties of BaFe_2As_2 and CaFe_2As_2 , two of the parent compounds for the iron arsenic high temperature superconductors. We find strong band back folding and hybridiza-

tion effects that lead to a reconstruction of the Fermi surface (FS) below the magnetic ordering temperature (T_N), which gives rise to a characteristic “flower-like” FS. We compare our data to itinerant spin model calculations and find them in reasonable agreement. These signatures of the magnetic ordering in the electronic structure vary significantly with value of the k_z momentum with coupling between charge carriers and magnetism being strongest whenever an efficient low energy scattering between the Fermi surface sheets around two sets of Fermi surfaces is kinematically possible. This clearly demonstrates the role of interband magnetic scattering in the iron arsenides. We were able to identify long parallel segments along the k_z direction spanning nearly half of the Brillouin zone that may play an essential role in the emergence of magnetic order in these materials. More interestingly, we discovered long parallel segments of the Fermi surface within the $a - b$ plane. This new nesting vector is significantly shorter than the $(\pi/a, \pi/a)$ vector related to the magnetic order. We speculate that these nested parts of the Fermi surface may be a precursor of a failed CDW order predicted by renormalization group studies [16, 17].

Single crystals of BaFe_2As_2 and CaFe_2As_2 were grown out of a FeAs flux as well as Sn flux using conventional high-temperature solution growth techniques[13, 14, 15]. BaFe_2As_2 and CaFe_2As_2 undergo a tetragonal to orthorhombic structural transition simultaneously with a paramagnetic to antiferromagnetic transition below $T_S \simeq T_N \simeq 130\text{K}$ and 170K , respectively[3, 12, 14, 15]. ARPES data were measured at the SIS beamline of Swiss Light Source, Switzerland, the beamlines 7.0.1 of the Advanced Light Source (ALS), USA, using a Scienta R4000 analyzer and Ames Laboratory using a Scienta SES2002

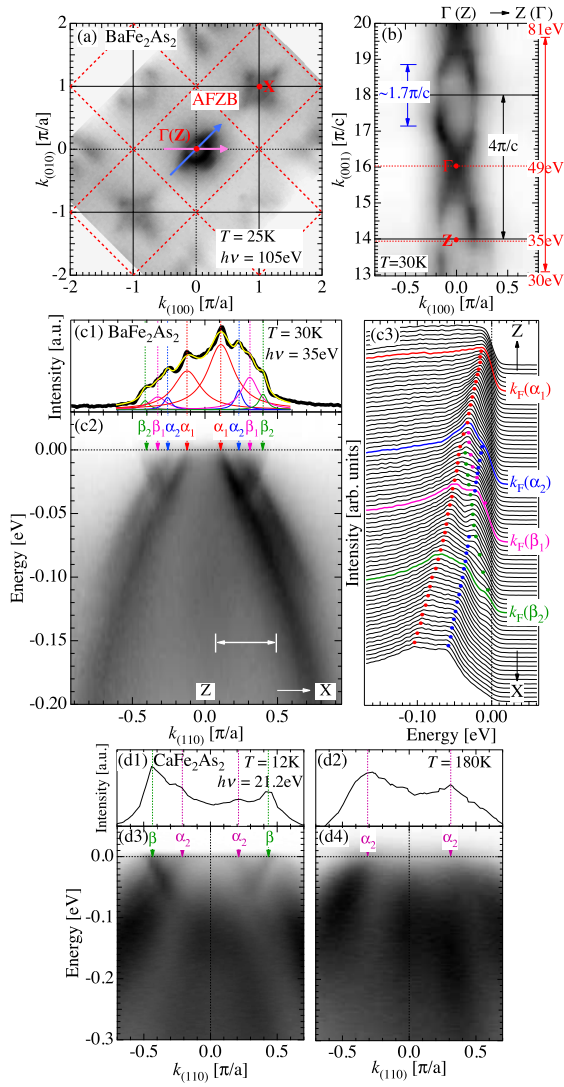


FIG. 1: (Color online) (a-c) BaFe_2As_2 and (d) CaFe_2As_2 data. FS map (a) along a - b and (b) along $k_{(001)}$ and $k_{(100)}$ (pink arrow in (a)). (Inner potential: $V_0 \equiv 13\text{eV}$) Blue arrow indicates the parallel segment. (c1) MDC of (c2) at Fermi energy (black curve) and the fitting curve (yellow). (c2) Band dispersion map along a diagonal cut (blue arrow in (a)). (c3) EDCs of (c2, a white arrow range). Colored circles follow hole-bands (α_1 and α_2) and electron-bands (β_1 and β_2). (d1-d2) MDC at Fermi level of (a3-b3). Band dispersion map along a diagonal cut (d3) below and (d4) above T_N .

with a Gammadata VUV5010 photon source. Energy and angular resolutions were 10 – 30meV and $\sim 0.1^\circ$, respectively. The high symmetry points X and Z for both two phases are defined to be $(\pi/a, \pi/a(b), 0)$ and $(0, 0, 2\pi/c)$, respectively, with k_x ($k_{(100)}$) and k_y ($k_{(010)}$) axes along the Fe-As bonds.

Band calculations predict two types of nearly circular FSs in the paramagnetic state: hole-like FSs centered at Γ (Z) and electron-like FSs centered at X[18, 19]. Below the magnetic ordering temperature one would expect

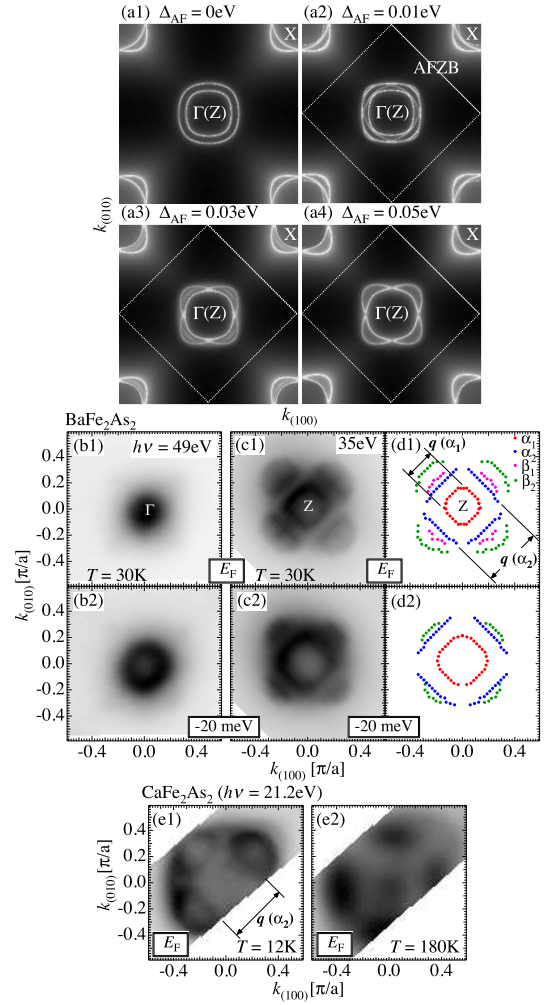


FIG. 2: (Color online) (a) Model calculation, (b-d) BaFe_2As_2 , and (e) CaFe_2As_2 data. (a1) Model FSs in non-magnetic phase. Reconstructed FSs for Δ_{AF} of (a2) 0.01 eV, (a3) 0.03 eV, and (a4) 0.05 eV. ARPES intensity about the Fermi energy and $E = -20\text{meV}$ obtained at (b1-b2) $h\nu = 49\text{eV}$ (near Γ) and (c1-c2) $h\nu = 35\text{eV}$ (near Z). (d1) FS and (d2) energy contour plots at $E = -20\text{meV}$ for $h\nu = 49\text{eV}$ data. FS map close to the zone center along a - b plane (e1) below and (e2) above T_N . Dimension arrows indicate nesting vector $q(\alpha_1) = 0.08(\pi/a, \pi/a)$ and $q(\alpha_2) = 0.32(\pi/a, \pi/a)$ for hole-band α_1 and α_2 , respectively.

back folding and hybridization of these bands leading to a reconstruction of the FS[19]. Figure 1 (a) shows a typical FS map from BaFe_2As_2 sample measured with 105 eV photons deep in the magnetically ordered state. Dark areas indicate the locations of the Fermi surfaces (FSs), which indeed display a more complicated structure than the one predicted in the paramagnetic state. To examine the character of the FSs, we show in Fig.1 (c2) an ARPES intensity along a diagonal direction (blue arrow in Fig.1 (a)) measured with 35eV photons. In addition to hole-like bands that are characteristic of the paramagnetic state, we observe electron-like bands that

are back folded from X-points about the antiferromagnetic zone boundary (AFZB, marked as red dashed lines in Fig.1(a)). The presence of multiple Fermi crossings is further verified by fitting of the momentum distribution curve (MDC) at Fermi level acquired along the same direction as shown in Fig. 1 (c1). The two hole-like bands (α_1 and α_2) and two electron-like bands (β_1 and β_2) can be also identified from the peak positions of energy distribution curves (EDCs) as marked with color circles in Fig.1 (c3). As shown in Fig. 2 (c1-d1), these bands hybridize leading to energy gaps (disconnected parts in the Fermi surface) and reconstruction of the Fermi surface. In order to compare the band structure between the magnetic and non-magnetic phase, we measured the ARPES data for CaFe_2As_2 deep below T_N ($T = 12\text{K}$) and slightly above T_N ($T = 180\text{K}$). The Fermi surface map near the zone center and the band dispersion map measured along a diagonal cut (blue arrow in Fig.1 (a)) are plotted in Fig. 2(e1) and Fig. 1(d3) for below T_N and Fig. 2(e2) and Fig. 1(d4) for above T_N . The data were measured with 21.2 eV photons. The electron band (β) is observed only below T_N (Fig. 1 (d3)), and it is absent above T_N (Fig. 1 (d2)). The associated “flower-like” shape of Fermi surface changes to nearly circular as expected from band calculations in non-magnetic phase.

We demonstrate that a simple model with the effect of band back folding about the AFZB reproduces many aspects of the data. Figure 2 (a1) shows a model of two hole- and electron-pockets surrounding the zone center and the corner, respectively, which are based on the band calculation for non-magnetic phase [20]. We assume that below T_N the states around Γ (or Z) are coupled to the states around X by an interband staggered mean field of magnitude Δ_{AF} via the mean field term in the Hamiltonian $\sum_{\mathbf{k},\sigma} \sigma \Delta_{\text{AF}} \left(d_{\mathbf{k},\sigma,\Gamma(Z)}^\dagger d_{\mathbf{k}+\mathbf{Q},\sigma,X} + h.c. \right)$, where σ refers to the spin and \mathbf{Q} is the magnetic ordering vector. Upon increase of Δ_{AF} from 10meV to 50meV, the conduction bands are increasingly folded back about the AFZB and the Fermi surfaces are reconstructed as shown in Fig.2(a2-a4) including twinning effects[21]. The degree of the reconstruction and hybridization gets stronger with increasing Δ_{AF} . Eventually the FS shape becomes “flower-like”. We plot the enlarged ARPES FS map of BaFe_2As_2 close to Γ and Z in Fig.2 (b1) and (c1), respectively, and the extracted Fermi crossing points for the latter in Fig.2 (d1). The experimentally observed “flower-like” FS is well reproduced by the simple model for Δ_{AF} of 50meV (Fig. 2(a4)). The reconstruction does not occur for k_z s where the interband coupling via the momentum \mathbf{Q} is not efficient (Fig. 2(b1)). Figure 2 (b2) and (c2) shows the ARPES intensity close to Γ and Z , respectively, slightly below the Fermi energy ($E = -20\text{meV}$). The band positions for the latter are plotted in Fig. 2 (d2). While the effect of band hybridization (“flower-like” shape) is clearly seen even in this en-

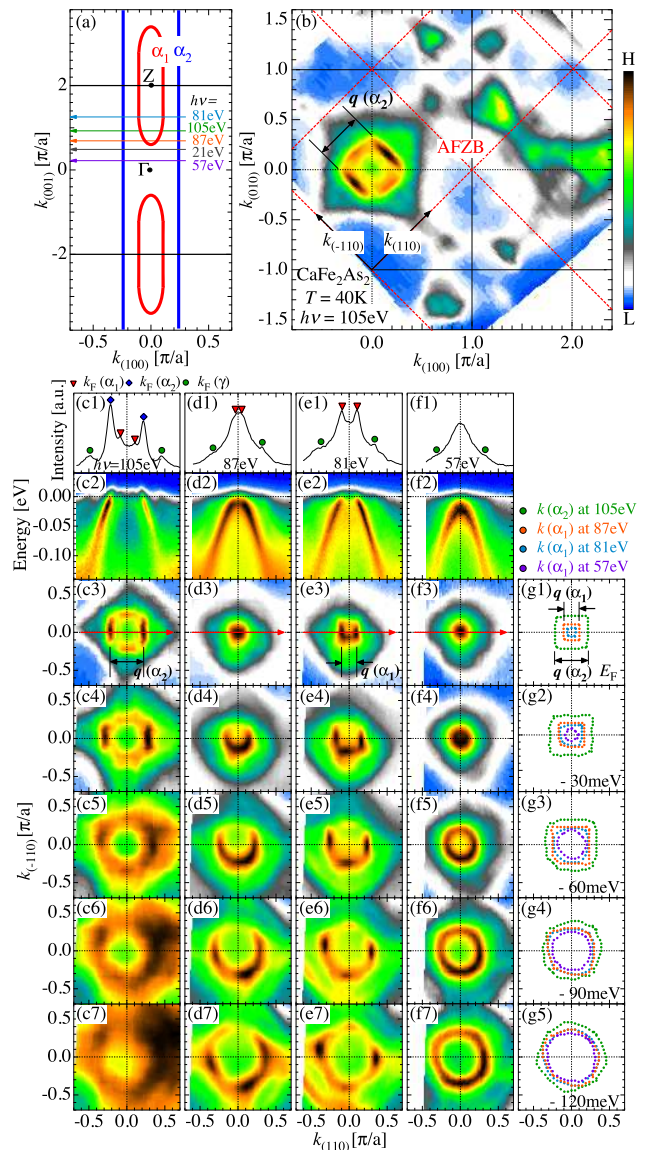


FIG. 3: (Color online) CaFe_2As_2 data at $T = 40\text{K}$. (a) Schematic FSs along $k_{(001)}$. (b) FS map along a - b plane. (c1)-(f1) MDC of (c2)-(f2) at the Fermi level. (c2)-(f2) Energy dispersion map measured along a red arrow in (c3)-(f3). ARPES intensity map about (c3)-(f3) Fermi level, (c4)-(f4) -30meV, (c5)-(f5) -60meV, (c6)-(f6) -90meV, and (c7)-(f7) -120meV. (g1)-(g5) FS and energy contour plots extracted from (c-f). Only stronger peaks between $k_F(\alpha_1)$ and $k_F(\alpha_2)$ are plotted. Dimension arrows indicate a nesting vector $q(\alpha_1)=0.07(\pi/a, \pi/a)$ and $q(\alpha_2)=0.31(\pi/a, \pi/a)$ of hole-band α_1 and α_2 , respectively.

ergy range around Z (Fig. 2(c2)), it is absent around Γ (Fig. 2(b2)) with a round shape of the energy contour. The coupling between charge carriers and magnetism is therefore strongest whenever efficient low energy scattering between the two sets of FS is kinematically possible, demonstrating the role of interband magnetic scattering in the iron pnictides. Previous ARPES studies [22, 23]

demonstrated strong dispersion along the k_z direction. This raised a question about the origin of magnetic order and pairing, since the presence of strong k_z dispersion would significantly limit in-plane $(\pi/a, \pi/a)$ nesting. By acquiring high quality data (Fig. 1(b)), we could see that, despite strong 3D-like dispersion, the Fermi surface has a long ($\sim 1.7\pi/c$) parallel segments along the k_z . The strong FS reconstruction discussed above is most prominent in this k_z range. It might be essential for nesting conditions leading to the emergence of the $(\pi/a, \pi/a)$ magnetic order and superconductivity.

Perhaps the most interesting experimental observation in our data is an incommensurate FS nesting (long parallel segments of FS in the $a-b$ plane seen in Fig. 2 (d1) for BaFe_2As_2 and (e1) for CaFe_2As_2), which doesn't appear in the result of the model calculation (Fig.2 (a4)). The nesting vector $q(\alpha_1) \simeq 0.1(\pi/a, \pi/a)$ and $q(\alpha_2) \simeq 0.3(\pi/a, \pi/a)$ for hole-band α_1 and α_2 , respectively, does not correspond to any previously reported density wave states. Therefore, we speculate that the gapless, nested Fermi surface may be a precursor of a failed density wave order such as the CDW predicted by renormalization group studies [16, 17]. In order to investigate the k_z variation of the FS nesting, we measured FS maps along $a-b$ for CaFe_2As_2 at various photon energies ($h\nu$ s). Figure 3(b) shows a typical FS map measured over a wide Brillouin zone with 105eV photons. The reconstructed “flower-like” FS and the significant nesting with $q(\alpha_2) \simeq 0.3(\pi/a, \pi/a)$ are clearly observed. In Fig. 3 (c3)-(f3), we plot FS maps focused on the zone center ($\Gamma(Z)$) measured at various $h\nu$ s. The k_z s corresponding to these photon energies are indicated in Fig. 3 (a) with the 1st Brillouin zone and schematic FSs of hole-bands (α_1 and α_2). We note that the intensity of several bands (α_1 , α_2 , and γ [22]) dramatically changes with photon energy, and the electron bands (β_1 and β_2) are absent due to matrix element effect. These are confirmed in the MDCs at the Fermi level shown in Fig. 3 (c1-f1) - the α_2 is most intense at 105 eV, while the α_1 is for 87eV, 81eV and 57eV photons. We also plot energy contour intensities in (c4)-(f4), (c5)-(f5), and (c6)-(f6) ($E = -30\text{meV}$, -60meV , -90meV and -120meV , respectively), which help us to understand how these bands behave with the binding energy. We found that the signature of band reconstruction is absent at specific k_z where the band doesn't cross E_F (Fig.3 (f1)-(f7)), and quickly evolved when the Fermi pockets starts appearing. This indicates that the band hybridization in the magnetic phase occurs only when the Fermi pockets overlap with folding-back bands and the gap opens with the consequent energy gain at the overlapped segments (seen as disconnected parts in Fig.1(c1) and (d1)). The parallel segments in the energy contours are significant up to $E \simeq -100\text{meV}$. This binding energy seems to agree with the energy bottom of electron-band back folded from the zone corner (see Fig. 1 (d3)). This indicates that the failed density wave order

is tied to the existence of magnetic long range order, and suggest a strong coupling between the staggered magnetization and other density wave order parameters in the iron pnictides.

In conclusion, we find strong band back folding and hybridization effects that lead to a reconstruction of the Fermi surface (FS) below the magnetic ordering temperature (T_N). The round hole-pockets observed above T_N evolve into a square shape surrounded by “flower petal” electron pockets below T_N . The FS data can be reasonably understood within a simple model of magnetic ordering. More interestingly, we find long parallel segments of the Fermi surface in the $a-b$ plane, which is not expected by the simple model. We speculate that these nested parts of the Fermi surface may be a precursor of a failed density wave order such as the CDW predicted by renormalization group studies [16, 17]. These findings demonstrate the complexity of these newly discovered materials and form the foundation of understanding the electronic properties that lead to high temperature superconductivity in the carrier-doped phase.

We thank A. Kreyssig, A. I. Goldman and B. N. Harmon for insightful discussions. ALS is operated by the US DOE under Contract No. DE-AC03-76SF00098. Ames Laboratory was supported by the US DOE - Basic Energy Sciences under Contract No. DE-AC02-07CH11358.

-
- [1] Y. Kamihara, T. Watanabe, M. Hirano, and H. Hosono, *J. Am. Chem. Soc.* **130**, 3296 (2008).
 - [2] C. de la Cruz *et al.*, *Nature (London)* **453**, 899 (2008).
 - [3] A. I. Goldman *et al.*, *Phys. Rev. B* **78**, 100506(R) (2008).
 - [4] R. J. McQueeney *et al.*, *Phys. Rev. Lett.* **101**, 227205 (2008).
 - [5] L. X. Yang *et al.*, *Phys. Rev. Lett.* **102**, 107002 (2009).
 - [6] D. Hsieh *et al.*, arXiv:0812.2289 (2008).
 - [7] S. O. Diallo *et al.*, arXiv:0901.3784v1 (2009).
 - [8] G. Liu *et al.*, arXiv:0904.0677v1 (2008).
 - [9] D. Vaknin *et al.*, *Phys. Rev. Lett.* **58**, 2802 (1987).
 - [10] H. Matsui *et al.*, *Phys. Rev. Lett.* **94**, 047005 (2005).
 - [11] P. Richard *et al.*, *Phys. Rev. Lett.* **99**, 157002 (2007).
 - [12] M. Rotter, *et al.*, *Phys. Rev. B* **78**, 020503(R) (2008).
 - [13] N. Ni *et al.*, *Phys. Rev. B* **78**, 014507 (2008).
 - [14] N. Ni *et al.*, *Phys. Rev. B* **78**, 014523 (2008).
 - [15] N. Ni *et al.*, *Phys. Rev. B* **78**, 214515 (2008).
 - [16] F. Wang, H. Zhai, Y. Ran, A. Vishwanath, and D. H. Lee, *Phys. Rev. Lett.* **102**, 047005 (2009).
 - [17] D. H. Lee *et al.*, unpublished.
 - [18] C. Liu *et al.*, *Phys. Rev. Lett.* **101**, 177005 (2008).
 - [19] F. Ma, Z.-Y. Lu, and T. Xiang *et al.*, arXiv:0806.3526 (2008).
 - [20] R. Sknepnek, G. Samolyuk, Y.-B. Lee, and J. Schmalian, *Phys. Rev. B* **79**, 054511 (2009).
 - [21] M. A. Tanatar *et al.*, arXiv:0904.2337 (2009).
 - [22] C. Liu *et al.*, *Phys. Rev. Lett.* **102**, 167004 (2009).
 - [23] P. Vilmercati *et al.*, arXiv:0902.0756 (2008).